NJC

Accepted Manuscript

This is an *Accepted Manuscript*, which has been through the Royal Society of Chemistry peer review process and has been accepted for publication.

Accepted Manuscripts are published online shortly after acceptance, before technical editing, formatting and proof reading. Using this free service, authors can make their results available to the community, in citable form, before we publish the edited article. We will replace this *Accepted Manuscript* with the edited and formatted *Advance Article* as soon as it is available.

You can find more information about *Accepted Manuscripts* in the Information for Authors.

Please note that technical editing may introduce minor changes to the text and/or graphics, which may alter content. The journal's standard Terms & Conditions and the Ethical guidelines still apply. In no event shall the Royal Society of Chemistry be held responsible for any errors or omissions in this *Accepted Manuscript* or any consequences arising from the use of any information it contains.

ROYAL SOCIETY OF CHEMISTRY

www.rsc.org/njc

Triply phenoxo bridged Eu(III) and Sm(III) complexes with 2,6-diformyl-4-methylphenol-di(benzoylhydrazone) : Structure, spectra and biological study on human cell lines

Kuheli Das,[a] Soumendra Nandi,[a] Sudipa Mondal,[a] Tulin Askun,[b] Zerrin Cantürk,[c] Pinar Celikboyun,[b] Chiara Massera,[d] Eugenio Garribba,[e] Amitabha Datta,[*,f] Chittaranjan Sinha,[*,a] Takashiro Akitsu[g]

Two dinuclear lanthanide(III) complexes, $[M_2(HL)_3]$ (M = Sm(III) (**1**), Eu(III) (**2**); H_3L, 2,6-diformyl-4-methylphenol-di(benzoylhydrazone)) are generated in good yield and systematically characterised. Single crystal X-ray structure determination of $[Eu_2(HL)_3]$ (**2**) has confirmed the tricapped trigonal prismatic geometry of the N_3O_6 coordination environment around europium. Indeed, Eu(1) and Eu(2) are bridged by phenolato-O belonging to the *p*-cresol ring, by deprotonated 'enol' groups from the benzoyl hydrazide part and imine-N centres. Temperature dependent magnetic study suggests anti-ferromagnetic coupling between the two Eu(III) ions and magnetic moment varies 0.48 B.M. at 5 K to 3.03 B.M. at 300 K. EPR spectra confirm the anti-ferromagnetic coupling among Eu(III) and Sm(III) atoms. Both the complexes show emission in visible range. The ligand, H_3L and the complexes exhibit anti-mycobacterial activity against *M. tuberculosis* H37Rv (ATCC 27294) and *M. tuberculosis* H37Ra (ATCC 25177) strains. Molecular docking of H_3L with enoyl acyl carrier protein reductase of *M.Tuberculosis* $H37R_v$ (PDB ID: 4U0K) is examined and the best docked pose of H_3L shows one hydrogen bond with Thr196 (2.03 Å).

Keywords: Diformyl benzoylhydrazone, Sm(III) and Eu(III), tricapped trigonal prism, VTM, anti-mycobacterial activity, cytotoxicity, molecular docking

[a] Department of Chemistry, Inorganic Chemistry Section, Jadavpur University, Kolkata – 700032, India

[b] Department of Biology, Faculty of Sciences and Arts, University of Balikesir, Cagis Campus, 10145, Balikesir, Turkey

[c] Department of Pharmaceutical Microbiology, Pharmacy Faculty, Anadolu University , Yunusemre Campus, 26470, Eskisehir, Turkey

[d] Dipartimento di Chimica, Università degli Studi di Parma, Viale delle Scienze, 17/A, 43124, Parma, Italy

[e] Dipartimento di Chimica e Farmacia, and Centro Interdisciplinare per lo Sviluppo della Ricerca Biotecnologica e per lo Studio della Biodiversità della Sardegna, Università di Sassari, Via Vienna 2, I-07100 Sassari, Italy

[f] Department of Physics, Faculty of Sciences and Arts, University of Balikesir, Cagis Campus, 10145, Balikesir, Turkey

[g] Department of Chemistry, Faculty of Science, Tokyo University of Science 1-3 Kagurazaka, Shinjuku-ku, Tokyo 162-8601, Japan

*Corresponding author. Fax: +91-33-2413-7121.

E-mail: c_r_sinha@yahoo.com (C. Sinna) ; amitd_ju@yahoo.co.in (A. Datta)

Introduction

Binuclear metal complexes are effective molecular devices in catalysis, chemical and biomedical applications, and the concerned ligands capable of forming binuclear derivatives with different metal ions are therefore of great interest. Indeed, if the two metal centers present an unsaturated coordination environment, the resulting complex can be used as a receptor for a secondary species and serve as catalyst. In this way they can mimic many biological sites, especially those in which the two metals can cooperate to form an active center as, for example, in oxygen receptors, activators, and carriers.[1] The character of the two metal ions, their coordination requirements, and the distance between them are the key elements in assembling host species. In this context, recent emphasis has been placed on the detailed study of the properties of lanthanide-phenolato complexes because of their postulated involvement in a range of biological and catalytic processes,[2] molecular recognition, magnetic devices and luminescence properties.[3] Schiff bases, one of the widely utilized noncyclopentadienyl ligands in coordination chemistry of transition and lanthanide metals,[4] have the obvious advantages of ease of synthesis, low cost, a hard donor atom framework, and tunable steric and electronic effects. However, the structurally characterized amido lanthanide complexes supported by Schiff base ligands are rare,[5] although various amido lanthanide complexes stabilized by noncyclopentadienyl ligands, such as β-diketiminates,[6] diamidoligands,[7] and bridged bisphenolate,[8] have been synthesized. Studies involving the chelation and coordination of ligands derived from hydrazone to lanthanide centers containing flexible multidentate ligands have been an ongoing area of active research. In recent years, much attention has been given to the syntheses of acyclic ligands that can give

rise to mononuclear or dinuclear lanthanide complexes with interactions between the metal centers. It is known that a considerable amount of work has been done on complexes with hydrazones because of their ability to chelate with lanthanide ions.[9] Hydrazone lanthanide complexes can be used as electroluminescent devices[10] and structural probes.[11] The di-Schiff bases of 2,6-diformyl-4-methylphenol were first developed by Robson.[12] A related dithiosemicarbazone was used by Hoskins *et al.*[13] for the synthesis of transition-metal complexes. This type of ligand is known to form binuclear complexes bridged by two different groups, *i.e*. the endogenous phenolic oxygen and an exogenous groups such as hydroxide, alkoxide, halide, pseudohalide, carboxylate, or pyrazolate ion. As well as the practical advantage of relatively low cost, high abundance and low toxicity, the lanthanide elements have chemical features which make them attractive as components of reagents for chemists. The lanthanide complexes have mainly drawn attention because of their versatile applications in designing sensors[14] and bio-study.[15] Tuberculosis, an infectious and chronically bacterial disease, caused primarily by the bacillus *Mycobacterium tuberculosis* and rarely by *M.bovis* and *M.africanum,* effects lung (pulmonary TB) and even can spread to the other organs (extra pulmonary TB).[16] Millions children has died per year from this disease.[17] Mycobacteria resist (multidrug resistant or MDR-TB) to many of chemicals, disinfectants, antibiotics and chemo-therapeutical agents.[18] Synthetic chemistry research is now directed to explore the synergistic relations between natural products and synthetic drugs for better treatment.

With this purpose, our strategy is to employ a multidentate ligand, 2,6-diformyl-4-methylphenol-di(benzoylhydrazone) (H_3L),[19] to synthesize lanthanide(III) complexes. Herein, we report dinuclear Sm(III) and Eu(III) complexes, $[Sm_2(HL)_3]$ (**1**) and $[Eu_2(HL)_3]$ (**2**). Both the complexes are systematically characterized and show

emission both in solution and solid phases. The solid state structure of complex **2** is investigated through X-ray diffraction analysis. The ligand and the complexes exhibit anti-mycobacterial activity on *M. tuberculosis* H37Rv (ATCC 27294) and *M. tuberculosis* H37Ra (ATCC 25177) strains. The activity of these molecules on three cancer cell lines, namely A549, MCF-7 and Caco-2, show moderate activity; with the best activity being observed for H_3L towards the A549 cell line. The anti-micobacterial efficiency of H_3L is examined by molecular docking with the enoyl acyl carrier protein reductase of *M.Tuberculosis* $H37R_v$ (PDB ID: 4U0K) and has been compared with the first line drug isoniazide.

Experimental

Materials

The binucleating hydrazone ligand was synthesized by reported procedure.[19] All chemicals and solvents were of reagent grade and used as received. $SmCl_3 \cdot 6H_2O$ and $EuCl_3 \cdot 6H_2O$ were purchased from Merck, India. Benzhydrazide and *p*-cresol were purchased from Fluka, India.

Physical measurements

Microanalytical data (C, H, and N) were collected on Perkin–Elmer 2400 CHNS/O elemental analyzer. Spectroscopic data were obtained using the following instruments: FTIR spectra (4000–400 cm^{-1}) by Perkin–Elmer FT-IR spectrophotometer model RX-1; UV–Vis spectra by Perkin–Elmer UV–Vis spectrophotometer model Lambda 25; the ^1H NMR spectra by Bruker (AC) 300 MHz FTNMR spectrometer. Emission was examined by LS 55 Perkin–Elmer spectrofluorimeter at room temperature (298 K) in CH_3CN solution under degassed

condition. The fluorescence quantum yield of the complexes was determined using anthracene as a reference with known Φ_R of 0.27 in ethanol.[20] The complex and the reference dye were excited at same wavelength, maintaining nearly equal absorbance (~0.1), and the emission spectra were recorded. The area of the emission spectrum was integrated using the software available in the instrument and the quantum yield is calculated according to the following equation:

$$\phi_s / \phi_R = \left[A_S / A_R \right] \times \left[(Abs)_R / (Abs)_S \right] \times \left[\eta_S^2 / \eta_R^2 \right]$$

Here, Φ_S and Φ_R are the fluorescence quantum yield of the sample and reference, respectively. A_S and A_R are the area under the fluorescence spectra of the sample and the reference, respectively, $(Abs)_S$ and $(Abs)_R$ are the respective optical densities of the sample and the reference solution at the wavelength of excitation, and η_S and η_R are the values of refractive index for the respective solvent used for the sample and reference. Fluorescence lifetimes were measured using a time-resolved spectrofluorometer from IBH, UK. The instrument uses a picoseconds diode laser (NanoLed-03, 370 nm) as the excitation source and works on the principle of time-correlated single photon counting. EPR spectra were recorded from 0 to 10000 Gauss in the temperature range 77-298 K with an X-band (9.15 GHz) Varian E-9 spectrometer. The EPR parameters reported in the text were obtained by simulating the spectra with the computer program Bruker WinEPR SimFonia.[21] The magnetic properties were investigated with a Quantum Design MPMS-XL superconducting quantum interference device magnetometer (SQUID) at an applied field 0.5 T in a temperature range 5-300 K and at 5 K in a field range -5 - +5 T. Powder samples were

measured in a pharmaceutical cellulose capsule. ESI mass spectra were recorded on a micro mass Q-TOF mass spectrometer (serial no. YA 263).

Preparation of the complexes

Synthesis of $Sm_2[(\mu\text{-}OC_6H_2CH_3)\{2,6\text{-}(CH{=}N\text{-}N{=}C(O)(C_6H_5))(CH{=}N\text{-}NH\text{-}(C{=}O)(C_6H_5))\}]_3$ (1). A methanol solution (10 mL) of $SmCl_3{\cdot}6H_2O$ (0.730 g; 2 mmol) was added to the solution of H_3L (1.20 g; 3 mmol) in the same solvent (40 mL) under stirring condition. The resulting yellow solution was kept undisturbed at room temperature for three days. Yellow rectangular-shaped crystals of **1** were obtained. Yield: 59% (0.884 g). Anal. Calc. for $C_{69}H_{54}N_{12}O_9Sm_2$: C, 53.66; H, 3.53; N, 10.89. Found: C, 53.52; H, 3.64; N, 10.74%. FTIR (KBr cm^{-1}): 3450 (br,w) 3270 (s), 1685 (s), 1611 (s), 1388 (s), 1266 (m), 1070 (s) 956 (m), 598 (w) 442 (w). ESI-MS (m/z): 1495.0 (10%) $[Sm_2(HL)_3]^+$.

Synthesis of $Eu_2[(\mu\text{-}OC_6H_2CH_3)\{2,6\text{-}(CH{=}N\text{-}N{=}C(O)(C_6H_5))(CH{=}N\text{-}NH\text{-}(C{=}O)(C_6H_5))\}]_3$ (2). A methanol solution (10 mL) of $EuCl_3{\cdot}6H_2O$ (0.732 g; 2 mmol) was added to the solution of H_3L (1.20 g, 3 mmol) in the same solvent (40 mL) under stirring condition. The resulting yellow solution was kept undisturbed at room temperature. Yellow rectangular-shaped single crystals of **2** were obtained after a week. These were isolated by filtration and air-dried before X-ray diffraction analysis. Yield: 62% (0.929 g). Anal. Calc. For $C_{69}H_{54}N_{12}O_9Eu_2{\cdot}8/3\ H_2O$: C, 53.52; H, 3.84; N, 10.86. Found: C, 53.64; H, 3.78; N, 10.95%. FTIR (KBr cm^{-1}): 3430 (br,w) 3200 (w), 2936 (s), 1616 (s), 1565 (s), 1382 (s), 1318 (m), 1082 (m) 706 (m), 598 (w) 468(w). ESI-MS (m/z): 1499.4 (100%) $[Eu_2(HL)_3]^+$.

Anti-MRSA activity

Preparation of samples for stock solution. The samples used in the study were weighed to 0.03 g and solubilized within 3 mL DMSO to prepare the main stock concentration of 10 mg/mL. The dilutions for sensitivity assays were prepared from the main stock.

Preparation of bacterial culture and inocula. Methicillin resistant *Staphylococcus aureus* (ATCC 33592) was used. In vitro antibacterial activity assays were determined by using Mueller Hinton Agar and Mueller Hinton Broth. Fresh cultures of bacteria (24 hours) on nutrient agar (NA) plates were suspended in sterile saline solution until the turbidity was equal to a 0.5 McFarland standard of 10^8 colony forming units (CFU) per mL,[22] then diluted at 100 times to reach of 10^6 CFU/mL.

Antibacterial activity assessment. Mueller Hinton Broth was used for micro-dilution assays for bacteria. The first well was filled with 190 µL and the remaining wells were filled with 100 µL of Mueller Hinton Broth. Extract (10 µL) was added to the first well, after mixing by pipetting several times, 100 µL of broth were transferred to the next well. Three-fold dilutions were performed from the first well to the next well (100 µL). This procedure was repeated to get serial dilutions until the final extract concentrations in the wells remained between 512 µg/mL and 1 µg/mL excluding the positive and negative control wells. The inoculum (20 µL) was added to all the wells except (-) control wells. The extract was not added to the (+) control wells. All micro-plates were incubated at 37 °C for 24-48 hours for bacteria.

Determination of minimal inhibitory concentrations (MICs). Thiazolyl Blue Tetrazolium Bromide (20 µL, Sigma) was added to the bacterial growth control wells (without extract) and the microplates were incubated at 37°C for an additional 2-4 hours. If the dye turned to pink (indicating positive bacterial growth); then Thiazolyl Blue Tetrazolium Bromide solution was added to the other wells to determine the MIC values. All tests were performed in triplicate. Methods for Determining Bactericidal Activity of Antimicrobial Agents were performed according to National Committee for Clinical Laboratory Standards for bacteria (NCCLS M26-A).[23]

Determination of minimal bactericidal activity (MBCs). To determine the minimum bactericidal concentrations (MBCs), fresh Mueller Hinton broth culture (185 µL) was transferred to each well, then15 µL of a bacterial suspension were added to the wells starting from MIC concentration values and proceeding to higher concentration wells in order to determine the minimum bactericide concentration (MBC).

Anti-mycobacterial activity

Microorganisms and culture media. *Mycobacterium tuberculosis* H37Ra (ATCC 25177) and *M. tuberculosis* H37Rv (ATCC 27294) were obtained from patient from hospital and used for antimycobacterial bioassays. Middlebrook 7H9 Broth and Middlebrook 7H10 Agar [24] were used as mycobacterial culture media.

Preparation of mycobacterial inocula. All strains were grown at 37°C in MGIT (Mycobacteria Growth Indicator Tubes) containing 4 mL of modified Middlebrook 7H9 Broth Base. OADC supplement (0.5 mL) (a mixture of oleic acid, albumin,

dextrose and catalase) and PANTA (0.1 mL) (an antibiotic mixture of Polymixin, Amphotericin B, Naladixic acid, Trimethoprim and Azlocillin) was added to each tube. Inoculum was prepared from a positive BACTEC Mycobacteria Growth Indicator Tube (MGIT) according to the manufacturer instructions.[24] To prepare inoculum from a positive BACTEC MGIT tube, the positive tubes were used beginning from the day after it first became positive (day 1 positive) up to and including the fifth day (day 5 positive). The positive tubes older than five days were cultured into fresh growth-medium. The tubes which were day-1 and day-2 positive proceeded to the inoculation procedure for the susceptibility test. The tubes between day 3 and day 5 positive were diluted using a 1 mL of the positive broth with 4 mL of sterile saline, to reach a total volume of 5 mL; this diluted suspension was then used for inoculation procedures. Inocula prepared from a Day 1 to Day 5 positive MGIT 7 mL tube range were between 0.8×10^5 and 3.2×10^5 CFU/mL. Each assay was performed according to the MGIT manual Fluorometric susceptibility test procedure recommended by manufacturer company. [24-26]

Antimycobacterial activity test. The mycobacterial activity of all extracts was tested using the Microplate Presto Blue Assay (MPBA). The test was performed in 96-well sterile microplates. All wells were filled with 100 µL of modified Middlebrook 7H9 broth. A 90 µL of modified Middlebrook 7H9 broth and 10 µL of BL were added to the first column of each row. Using a multi-channel pipette serial, three-fold dilutions were made down to the desired minimum concentration. Then, 20 µL of *M. tuberculosis* inoculum was added to the wells (except to the negative control well). Final concentrations in the range of 1-512 µg/mL were obtained. Each microplate was incubated for 5 days at 37 °C. After incubation, 20 µL of Presto blue solution

(Invitrogen, Life Technologies) was added to one positive control well and the micro-plates were re-incubated. After that, if the positive well color turned to pink, all the other wells were processed in the same way. Blue and pink colors in the wells indicate no growth and growth, respectively. The minimal inhibitory concentration (MIC) was defined as the lowest concentration of the extracts that gives a negative result (by preventing the color change to pink). For determining the minimal bactericidal concentration (MBC), wells with no growth (20 μL) were transferred to new plates containing 80 μl of fresh modified Middlebrook 7H9 broth and processed MPBA.

Cell viability / Cytotoxicity assay

Cell culture. A549 (non-small cell lung cancer); MCF-7 (breast cancer); Caco-2 (colon cancer cell line) and healthy cell lines 3T3 (Mouse embryo fibroblast), which were used in the study, were provided from the ATCC cell bank. The cells were grown in a RPMI 1640 medium supplemented with 2 mM L-glutamine, 10% fetal-bovine serum and 1% penicillin-streptomycin at a temperature of 37^{o}C in a humidified incubator with a 5% CO_2 atmosphere. Cytotoxicity was studied following the WST-1 procedure.

WST-1 assay. The ligand H_3L, complexes **1** and **2** of concentrations 500, 250, 125, 62.5, 31.25, 15.625, 7.8125, 3.9, 1.95, 0.97 μg/mL were seeded in 5×10^3 cells which were cultivated in each well of a 96-well plate. After 24 hours of incubation, 0.1 mL of WST-1 working solution was added to each well and they were incubated at 37 °C in a 5 % CO_2 incubator for 3-4 hours. The absorbance intensity of the living cell in the plate was read in a ELISA device (Cytation3, Biotek, USA) at 450 nm. The acquired absorbance values corresponded to the metabolic activities of the cells in the culture.

Because this value was correlated to the number of living cells, the results were expressed in liveliness percent and calculated using the formula below.

$$Liveliness\ percent = \frac{100}{Absorbance\ of\ the\ control / Absorbance\ of\ the\ sample}$$

Docking studies

Molecular docking is used to envisage the interaction of small molecules with proteins. The crystal structure of the protein of interest may be collected from PDB (Protein Data Bank) and the target molecule can be placed into the protein structure; the best doc pose is then calculated following docking score, LogP, number of hydrogen bond donors and acceptors etc. as per Lipniski's rule of five.[27,28] In this work, the crystal structure of the enoyl acyl carrier protein reductase of *M. tuberculosis* H37Rv was downloaded from the RCSB protein data bank (http://www.pdb.org) and used for docking. The protein (PDB id: 4U0K) was co-crystallized with (3S)-N-(5-chloro-2-methylphenyl)-1-cyclohexyl-5-oxopyrrolidine-3-carboxamide and nicotinamide-adenine-dinucleotide. *In silico* docking studies were performed using the CDOCKER module of the Receptor-Ligand interactions protocol section of Discovery Studio client 3.5.[29] Initially a pretreatment process for both the protein and the ligand was carried out. The crystal structure of H_3L was directly used for docking but for isoniazide the structure was drawn in Chemdraw 5.0, saved in .mol file and imported to the Discovery studio 4.0 platform. The Ligand and Protein preparation were carried out separately using the Prepare Ligand module and Prepare Protein module tool of Discovery studio 4.0. The existing ligand was removed from the PDB structure and substituted with the prepared ligand. The most favorable

docked pose was selected according to the minimum free energy of the protein-ligand complex and was subsequently analyzed to investigate the interactions involved.

ADMET prediction

Absorption, distribution, metabolism, excretion and toxicity (ADMET) predictions were done in the ADMET descriptor module of the Small molecules protocol of Discovery studio client 4.0. The druglikeness of the compounds were checked too following Lipniski's rule of five.[27,28]

X-ray crystallography

The crystals of $[Sm_2(HL)_3]$ (**1**) and $[Eu_2(HL)_3]$ (**2**) were grown by slow evaporation of the synthetic reaction mixture. However, crystals of **1** underwent rapid degradation and X-ray diffraction data could not be collected even in sealed tube. Crystal data and experimental details for data collection and structure refinement for **2** are reported in **Table 1**. Intensity data and cell parameters were recorded at 298(2) K on a Bruker APEX II (MoKα radiation λ = 0.71073 Å) equipped with a CCD area detector and a graphite monochromator. The raw frame data were processed using SAINT and SADABS to yield the reflection data file.[30] The structure was solved by Direct Methods using the SIR97 program[31] and refined on F_o^2 by full-matrix least-squares procedures, using the SHELXL-97 program[32] in the WinGX suite v.1.80.05.[33] All non-hydrogen atoms were refined with anisotropic atomic displacements. The hydrogen atoms were included in the refinement at idealized geometry (C-H 0.95 Å) and refined "riding" on the corresponding parent atoms. The weighting scheme used

in the last cycle of refinement was $w = 1/ [\sigma^2 F_o^2 + (0.0947P)^2 + 7.3450P]$, where $P = (F_o^2 + 2F_c^2)/3$.

Table 1. Crystal data and structure refinement information for **2**.

Compound	**2**
Formula	$C_{69}H_{54}N_{12}O_9Eu_2 \cdot 8/3\ H_2O$
FW	1547.20
Crystal system	Monoclinic
Space group	*C2/c*
a (Å)	46.333(3)
b (Å)	17.2990(10)
c (Å)	32.343(2)
β (º)	132.486(7)
V (Å^3)	21606(2)
Z	12
T (K)	298(2)
ρ (g cm^{-3})	1.427
μ (mm^{-1})	1.791
F(000)	9320
Total reflections	129889
Unique reflections (R_{int})	22113 (0.0949)
Observed reflections [$F_o>4\sigma(F_o)$]	13946
GOF on F^{2a}	1.031
R indices [$F_o>4\sigma(F_o)$]^b R_1, wR_2	0.0534, 0.1452
Largest diff. peak and hole (eÅ^{-3})	1.302, -0.918

[a]Goodness-of-fit S = $[\Sigma w(F_o^2-F_c^2)^2/ (n-p)]1/2$, where n is the number of reflections and p the number of parameters. [b]$R_1 = \Sigma \| F_o | - | F_c \| / \Sigma | F_o |$, $wR_2 = [\Sigma[w(F_o^2-F_c^2)^2]/\Sigma[w(F_o^2)^2]]^{1/2}$.

Results and discussion

Synthesis and formulation

2,6-Diformyl-4-methylphenol-di(benzoylhydrazone), H_3L, was obtained by reacting 4-methyl phenol with *para*-formaldehyde and hexamethylene tetraamine in strongly acidic medium followed by the condensation with benzhydrazide.[19] $SmCl_3 \cdot 6H_2O$ / $EuCl_3 \cdot 6H_2O$ were then reacted with H_3L (2:3 molar ratio) under refluxing condition in methanol and the products were isolated on cooling the reaction mixture. The complexes were re-crystallized from methanol; their composition, $[M_2(HL)_3]$ (M = Sm (**1**), Eu (**2**)) is supported by elemental analyses. The complexes are nonconducting. The structural confirmation has been achieved by single crystal X-ray diffraction of $[Eu_2(HL)_3]$. The crystals of **1** show rapid decomposition and the X-ray crystal structure could not be determined. Therefore, the structure is confirmed by mass spectral analysis which shows a peak at m/z, 1495.06 suggesting the presence of the dimeric ionic species $[Sm_2(HL)_3]^+$ (m/z, 1495) for complex **1** (**Figure S1**). For complex **2**, the corresponding peak is observed at 1499.39 which confirms the existence of $[Eu_2(HL)_3]^+$ (m/z, 1499.2) (**Figure S2**).

The IR spectrum of H_3L shows ν(C=O) and ν(C=N) bands at 1649 and 1547cm^{-1}. The ν(C=O) bands shift to *ca*. 1685 cm^{-1} for **1** and 1616 cm^{-1} for **2** due to coordination with metal centre. Similarly, the ν(C=N) bands shift to *ca*. 1611 and 1565 cm^{-1} in the complexes **1** and **2**, respectively.[34] In the complex the ligand is

bideprotonated and most likely present in the tautomeric form -C=N-NH-(C=O)-Ph (see the details in the crystal structure discussion); indeed, the -NH vibration frequency of free ligand appears at 3237 cm^{-1} while it is observed at 3270 and 3200 cm^{-1} for **1** and **2**, respectively. This tautomeric form is also supported by the absence of the sharp ν(OH) band typical of phenol groups at 3400 cm^{-1}.

Crystal structure of 2

Compound **2** is the dinuclear complex $[Eu_2(HL)_3]\cdot 8/3H_2O$, as elucidated by the crystal structure in **Figure 1.** Selected bond lengths and angles are listed in **Table 2**. The asymmetric unit consists of one whole complex, one half complex and four H_2O of crystallization. In each of the two independent complexes, the three V-shaped ligands are doubly deprotonated, with the single remaining hydrogen most likely located on the nitrogen atoms N2 or N4. This hydrogen could not be found in the difference Fourier map, but its presence is supported by the NH stretching IR data and by the existance in the ligand of C=O groups, (the bond distances C9-O2 and C17-O3 span from 1.236(9) to 1.279(7), and from 1.225(7) to 1.276(7), respectively. See also IR data). The ligands are pentadentate through three oxygen and two nitrogen atoms; more precisely, every "arm" of the V-shaped ligand comprises a NO chelating unit which forms a five-membered ring with one of the two metal centers, which are in turn bridged by the oxygen atoms O1 (**Figure 1a**). Each of the two Eu centers interacts with three distinct ligands (shown in blue, green and yellow in **Figure 1a**) through the μ_2-phenolate oxygen atoms O1 of the *p*-cresol ring, the deprotonated –OH groups of the benzhydrazide moiety and the imine-N atoms. The net result is a triple helical architecture in which the ligands coil around a pseudo-three fold axis passing

through the two europium atoms. Due to this spatial arrangement, the configuration of $[Eu_2(HL)_3]$ could be described either as Δ or Λ; however, since the complex crystallizes in a centro symmetric space group, both the entantiomers are present in the crystal structure. A N_3O_6 coordination environment about Eu(III) with a tricapped trigonal prismatic geometry leads to the formation of five membered (EuOCNN) and six membered (EuNCCCO) chelate rings. All the Eu–O and Eu–N bond lengths show normal values for such systems, in the range 2.342(5) - 2.477(6) and 2.593(6) - 2.693(5) Å, respectively. The angles of the phenoxido bridged metal atoms, namely Eu1–O1a–Eu2, Eu1–O1b–Eu2 and Eu1–O1c–Eu2 do not differ notably (**Table 2**). The Eu----Eu separation in the two independent units are 3.5973(7) and 3.5685(7) Å, respectively. In the lattice, the complexes interact one with the other through weak π···π stacking interactions involving the benzhydrazide phenyl rings of the ligands (**Figure 1b**). The centroid···centroid distance of 4.041(5) Å is slightly longer compared to the average value of 3.8 Å found for similar compounds.[35] The planes passing through the aromatic moieties involved in the stacking are tilted of 7.07(9)° one with respect to the other.

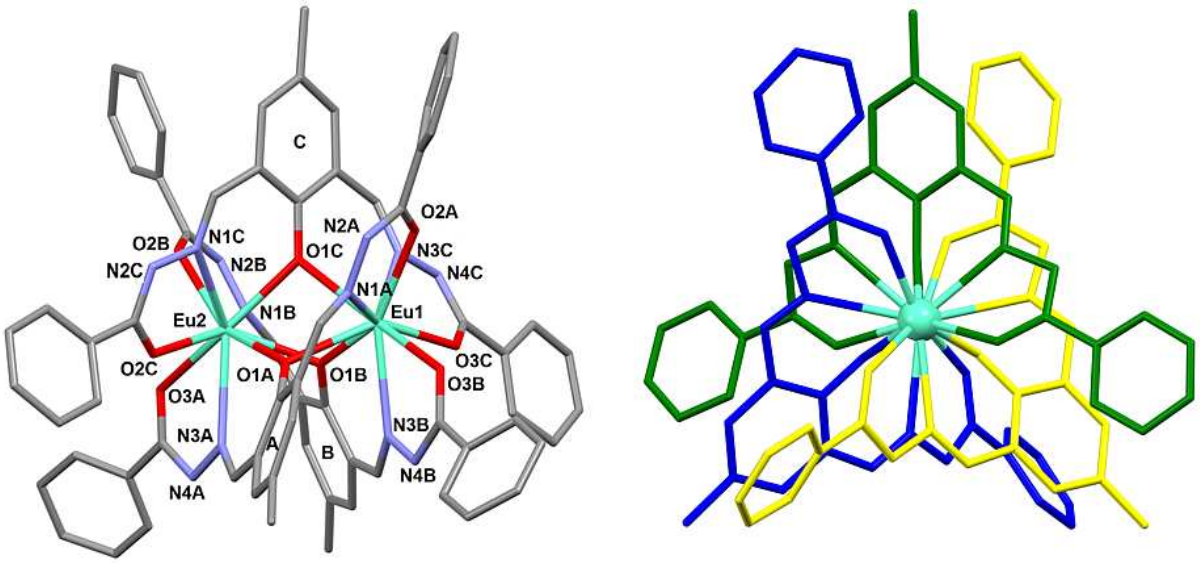

(a)

Figure 1. (a) Left: One of the two independent complexes $[Eu_2(HL)_3]$ (**2**) with the corresponding labeling scheme. The three ligands are labeled with A, B and C, respectively. Lattice water molecules and hydrogen atoms have been omitted for clarity. Right: View along the pseudo-threefold axis of the complex; the ligands are shown in blue, yellow and green and the europium ion is represented as light blue sphere.

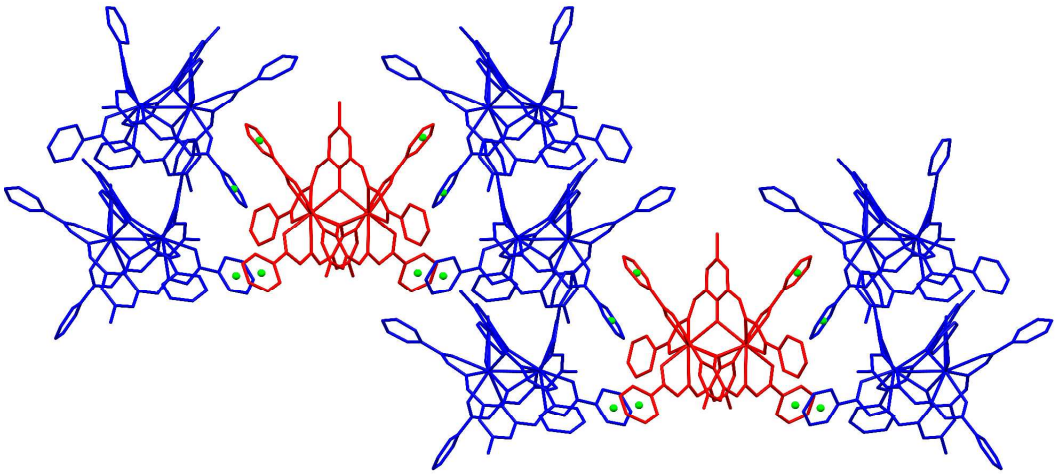

Figure 1. (b) Crystal packing along the c* axis of the unit cell. The two independent Eu complexes are in red and blue, respectively. The centroids of the aromatic rings involved in the weak π···π interactions are represented as green spheres.

Table 2. Selected bond lengths [Å] and angles [°] for **2**.

Eu1-Eu2	3.5973(7)	Eu2-N3A	2.675(5)	Eu3-O2D	2.3659(6)
Eu3-Eu3[b]	3.5685(7)	Eu2-O1A	2.387(6)	Eu3-N1E	2.5934(6)
Eu1-N1A	2.693(5)	Eu2-O3A	2.477(6)	Eu3-O1E	2.3564(4)
Eu1-O1A	2.424(6)	Eu2-N1B	2.629(5)	Eu3-O2E	2.3567(7)
Eu1-O2A	2.452(5)	Eu2-O1B	2.424(5)	Eu1-O1A-Eu2	96.8(2)
Eu1-N3B	2.614(5)	Eu2-O2B	2.342(5)	Eu1-O1B-Eu2	97.3(2)
Eu1-O1B	2.369(5)	Eu2-N1C	2.685(5)	Eu1-O1C-Eu2	100.3(2)
Eu1-O3B	2.441(6)	Eu2-O1C	2.344(5)	Eu3-O1D-Eu3[b]	97.7(2)
Eu1-N3C	2.615(5)	Eu2-O2C	2.396(5)	Eu3-O1E-Eu3[b]	98.5(2)
Eu1-O1C	2.342(5)	Eu3-N1D	2.682(6)		
Eu1-O3C	2.353(5)	Eu3-O1D	2.386(7)		

b:-x,+y,-z+1/2+1

Absorption and emission spectra

The absorption spectrum of H_3L shows intense ligand-centered (LC) bands at 302, 363 and 443 nm in dimethyl formamide. These bands are assigned to π→π* and n→π* transitions.[36] The LC band at 363 nm shifts to longer wavelengths in the complexes, namely to *ca*. 404 nm for $[Sm_2(HL)_3]$ (**1**), and to 400 nm for $[Eu_2(HL)_3]$ (**2**) (**Table 3**). On the other hand, the π→π* band at 303 nm remains almost

unchanged in the complexes. The molar extinction coefficients of the complexes (ε(dm^3 $mol^{-1}cm^{-1}$): **1**, 37356; **2**, 71,313) are much higher than those of H_3L (ε (dm^3 $mol^{-1}cm^{-1}$)**:** 6051) at 300 nm. Lanthanide ions containing 4*f* valence electrons show only minimal changes in electronic absorption spectra, such as small displacements in the peak positions usually towards longer wavelengths. Therefore no absorption bands are observed beyond 400 nm.

Photoluminescence studies of H_3L in DMF and of the complexes **1** and **2** in methanol were carried out at room temperature (**Figures 2a, 2b, 2c**). H_3L fluoresces upon excitation at 302 and 363 nm (**Table 3**) and the emission bands appear at 424 and 546 nm. No emission was found for H_3L on excitation at n→π* absorption band (443 nm). Both the complexes, **1** and **2**, show a significantly different emission when they are excited at the MLCT band maxima (>400 nm). Usually lanthanide salts are well known for emission in visible region. The excitation in the UV region shows very weak peaks with respect to the visible region. The Eu(III) complex shows emission at ~500 nm on excitation at 400 nm whereas the Sm(III) complex shows it at ~ 470 nm.

Table 3. UV-Vis, Fluorescence and Lifetime data of H_3L, $[Sm_2(HL)_3]$ (**1**) and $[Eu_2(HL)_3]$ (**2**).

Compd	UV-Vis spectral data λ_{max}(nm) 10^{-2} ∈ (dm^3 $mol^{-1}cm^{-1}$)	Fluorescence Data			Fluorescence Decay Data			
		λ_{ex} (nm)	λ_{em} (nm)	Φ	χ^2	τ (ns)	$k_r \times 10^{-7}$	$k_{nr} \times 10^{-9}$

H_3L	301 (60.7) 363 (23.5) 443 (1.6)	301 363	410, 522 424, 546	0.04	1.112	0.1	0.149	7.32
$[Sm_2(HL)_3]$ (**1**)	300 (374) 404 (149)	300 404	468 467	0.002	1.1286	0.07	8.2	13.6
$[Eu_2(HL)_3]$ (**2**)	300 (713) 400 (226)	300 400	497 497	0.01	1.1076	2	2.18	0.52

The emission studies of ligand and complexes were also carried out in the solid state (**Figures 2d, 2e, 2f**). The emission bands at solid phase appear at longer wavelength than that of solution phase. H_3L shows the strong emission band at 589 nm and a very weak band at 489 nm on excitation at 363 nm. The most common emission bands of europium(III) observed at 580 to 705 nm corresponding to deactivation of singlet excited state $^5D_0$ to ground state ^7F_J (J = 0-4) whereas the Sm (III) shows four emission peaks ranging from 560 to 721 nm, attributed to be the characteristic emission for the $^4G_{5/2} \rightarrow {}^6H_J$ (J = 5/2, 7/2, 9/2, 11/2).[37] In the present work, five luminescence peaks for $[Sm_2(HL)_3]$ are observed at 425, 489, 532, 602, 644 and 707 nm among which the strongest peak (*i.e.* 489 nm) may be generated due to ligand centered emission and the peak at 602, 644,707 nm are due to $^4G_{5/2} \rightarrow {}^6H_J$

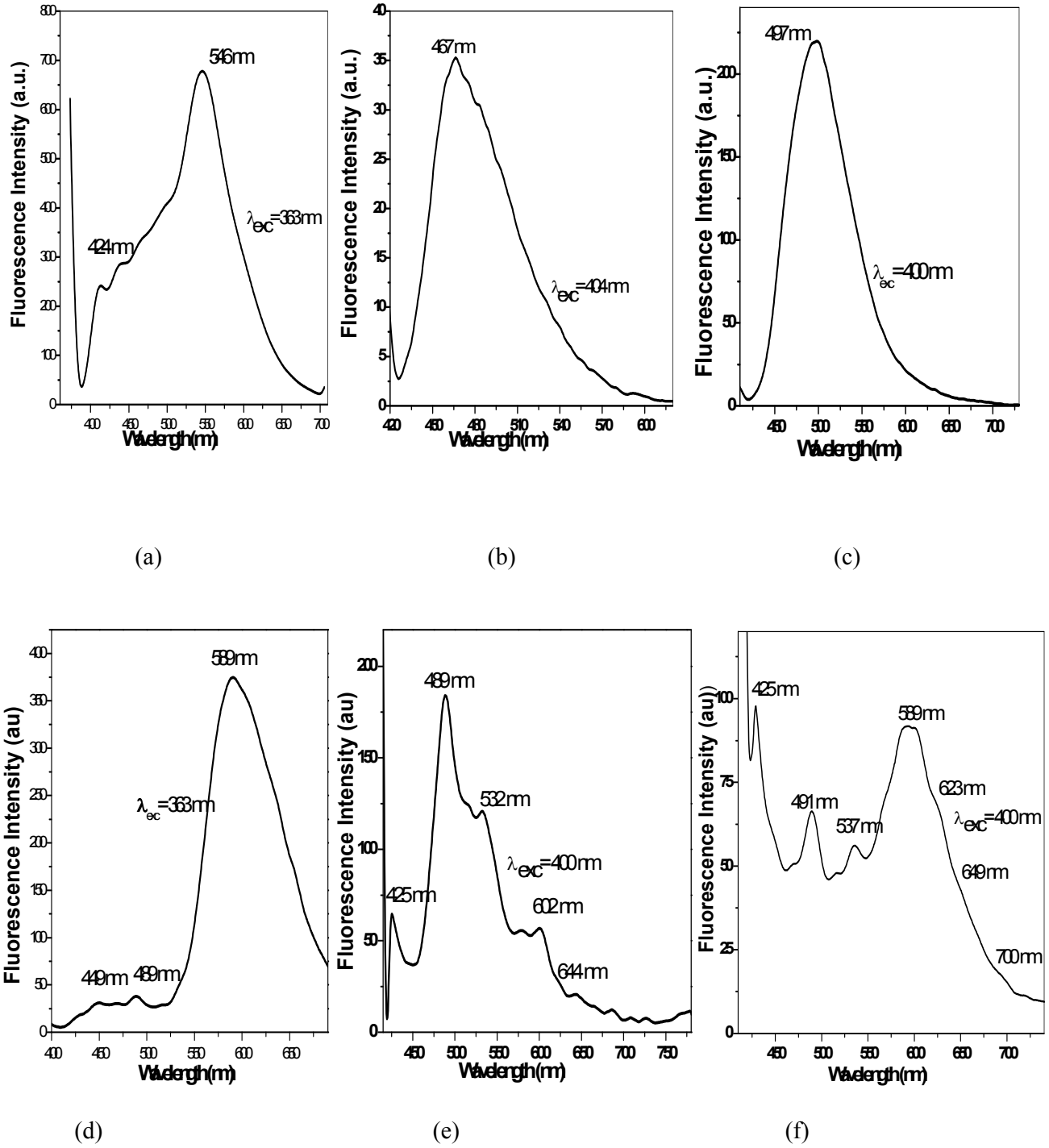

Figure 2. Emission spectra of (a) H_3L (in DMF), (b) Sm(III) complex (**1**) in MeOH,, (c) Eu(III) complex (**2**) in MeOH, and (d) H_3L, (e) Sm(III) complex (**1**), (f) Eu(III) complex (**2**) in the solid state.

(J=7/2, 9/2, 11/2). Similarly, in $[Eu_2(HL)_3]$ the corresponding strongest peak is observed at 589 nm along with rest three emission bands at 425, 491 and 537 nm. Additionally, few emission peaks are found for **2** at 623, 649 and 700 nm with very weak intensity which may be due to $^5D_0 \rightarrow {}^7F_J$ (J=2-4). Emission peaks reveals that contribution of metal ion is very negligible and that is why ligand centered bands are dominated in the present case. Basically photoluminescence of Ln^{3+} complexes upon excitation at ligand absorption bands arises from the metal dominated f-level. Consequently, the excited f-levels are populated as a result of energy transfer from the triplet state of ligand (L_T^*), which is generated by rapid intersystem crossing by the following way, $L_S^* \rightarrow L_T^* \rightarrow (Ln^{3+})_S^*$. For fluorescence, the energy of $(Ln^{3+})_S^*$ must be lower than $L(L_T^*)$. If the reverse happens or the energy gap between the two is very low, then energy transfer from Ln^{3+} to ligand is possible. It reduces the efficiency of fluorescence sensitivity. Besides, the energy transfer between the lanthanide ions is a non-radiative process, which may partially contributes to the quenching of the Ln^{3+} ions.[37] The fluorescence quantum yields were measured for all the compounds in solution state. In the case of H_3L the value is higher (ϕ = 0.04) than both the complexes **1** (ϕ = 0.002) and **2** (ϕ = 0.01) which is comparable with literature value.[37(c)] Emission from Ln(III) ions can often be quenched by high frequency vibrations of OH, CH, C=O or NH bonds in solvents (e.g. methanol, water, ethanol) or ligand framework.[38] The latter effect could actually be the reason for low quantum yields in this case.

The decay profile of H_3L and of its corresponding metal complexes (**1** and **2**) is shown in **Figure 3**. Lifetime data were taken on excitation at 370 nm. The fluorescence decay fits bi-exponential nature. Here we use mean fluorescence lifetime

(τ_f=$a_1\tau_1$+$a_2\tau_2$ where a_1 and a_2 are relative amplitudes of the decay process) to compare the excited state stability of the complexes. The radioactive and non-radioactive rate constants (kr and knr) were calculated and the data show knr values, which are unusually higher with respect to the kr ones (**Table 3**). [$Eu_2(HL)_3$] (**2**) shows higher lifetime (τ :~2 ns) than the free ligand (τ : 0.1 ns) whereas the lifetime of [$Sm_2(HL)_3$] (**1**) (τ :~0.07 ns) is quite lower. Though the literature value shows lanthanide complexes with high life time values in microsecond or millisecond range,[37] in present work, the lifetime of both the complexes belongs in nanosecond range. This is probably due to two main factor: (1) low energy difference between triplet state of ligand and emissive excited state of lanthanide ion which results back energy transfer to ligand triplet state and fluorescence efficiency as well as life time decreases drastically (2) excited state energy of the lanthanides is transferred as nonradiatively to lower energy lying O-H and N-H oscillators, leading to the substantial decrease of the lifetime.[38,39] Sm(III) complex shows extremely low value of life time may be due to the fact that the energy difference between excited state and ground state of Sm(III) complex is very less.

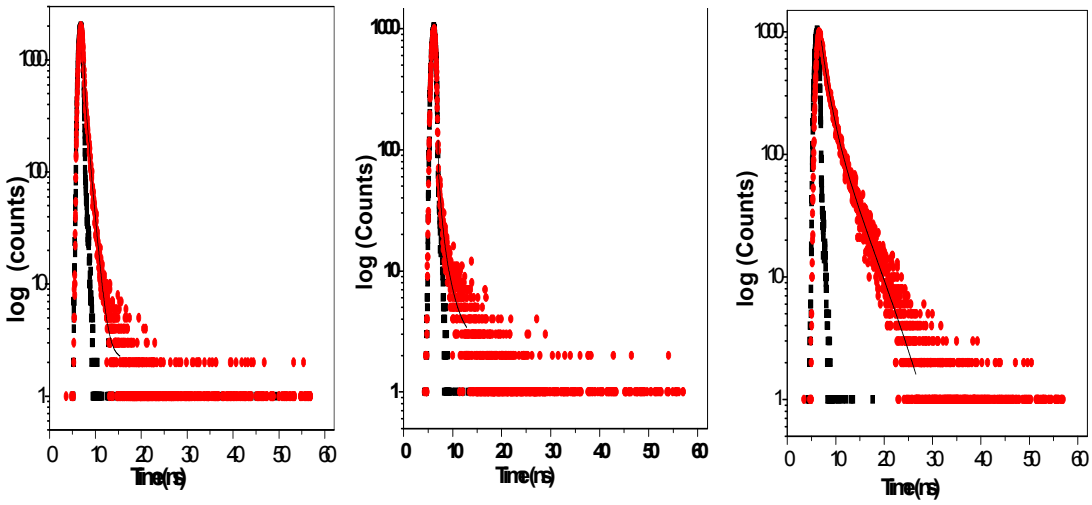

(a) (b) (c)

Figure 3. Exponential decay profile (•) and fitting curve (—) of H_3L(a), Sm(III) complex (**1**) (b) and Eu(III) complex (**2**) (c). Excitation is carried out at 370 nm.

EPR spectra

EPR spectra, recorded at room (298 K) or liquid nitrogen (77 K) temperature on the polycrystalline powder of **1** and **2**, are characterized by the absence of spectral signals in the range 0-8000 Gauss, indicating a diamagnetic behavior of Sm(III) or Eu(III) complexes (**Figures 4** and **5**). Such a behavior is consistent with the antiferromagnetic nature of **1** and **2** determined by VTM measurements. Only weak resonances centred around $g \sim 2$ (more evident for **1**) are detected. As observed for other metal complexes, for example Cu(II) compounds, in μ-phenoxo bridged species the angle M–O–M (M = metal ion) is critical: when this angle overcomes a threshold value, peculiar of each metal ion (it is ~77° for copper(II)[40]), the magnetic coupling changes from ferromagnetic to antiferromagnetic.[40,41] Even if, to the best of our knowledge, for Sm(III) and Eu(III) compounds no threshold angle for the transition from ferro- to antiferromagnetic coupling has been determined until now, the experimental Sm–O–Sm and Eu–O–Eu angles in **1** and **2** (in the range 96-101°) appear large enough to cause an antiferromagnetic interaction between the two metal ions. The diamagnetism of **1** and **2**, revealed by EPR spectroscopy, confirms these observations.

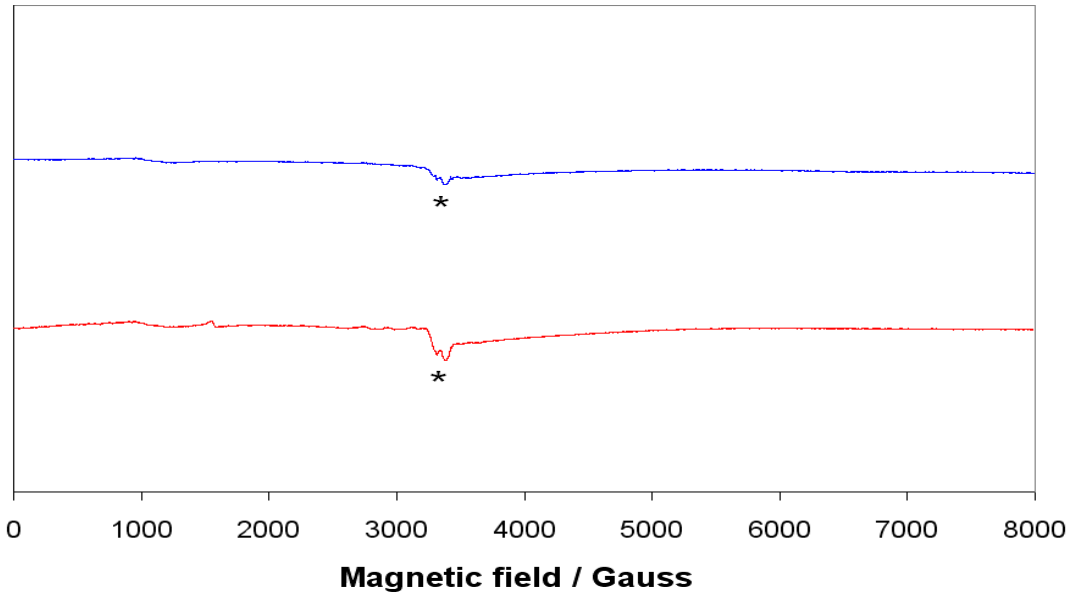

Figure 4. X-band EPR spectra of the polycrystalline complex **1**: RT (blue) and 77 K (red). The asterisk denotes the weak signal at $g \sim 2$.

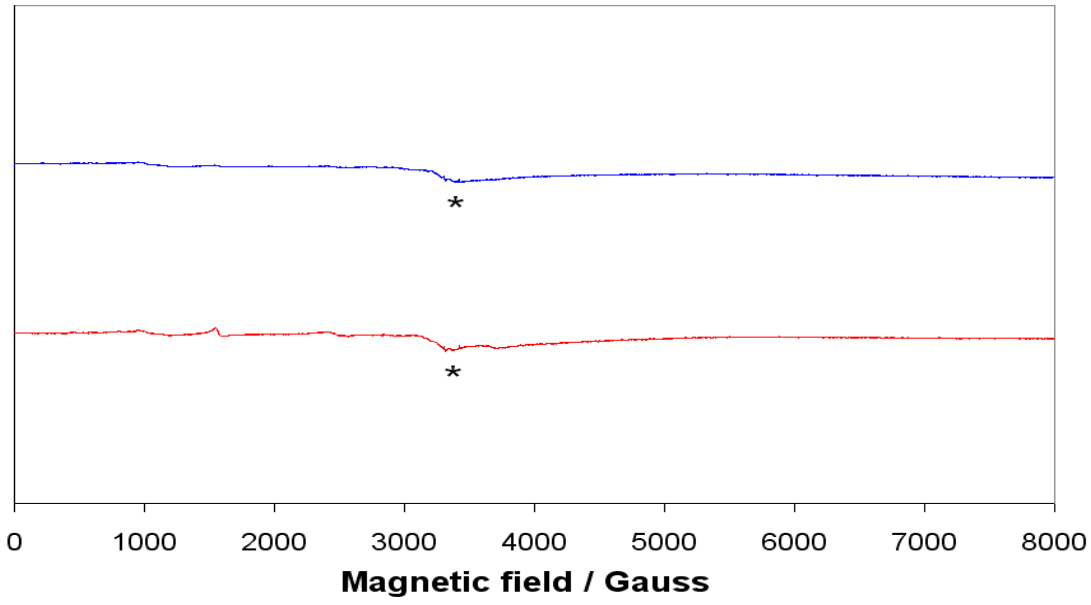

Figure 5. X-band EPR spectra of the polycrystalline complex **2**: RT (blue) and 77 K (red). The asterisk denotes the weak signal at $g \sim 2$.

In DMF, where they are fairly soluble, **1** and **2** show the same behaviour as in the solid state (**Figure 6**). The intensity of the EPR spectra is very weak, suggesting that the dinuclear arrangement is retained in this solvent. This appears to be in contrast with what observed for other polynuclear metal complexes, for example formed by Cu(II), which in a coordinating solvent dissociate to give the mononuclear form.[42]

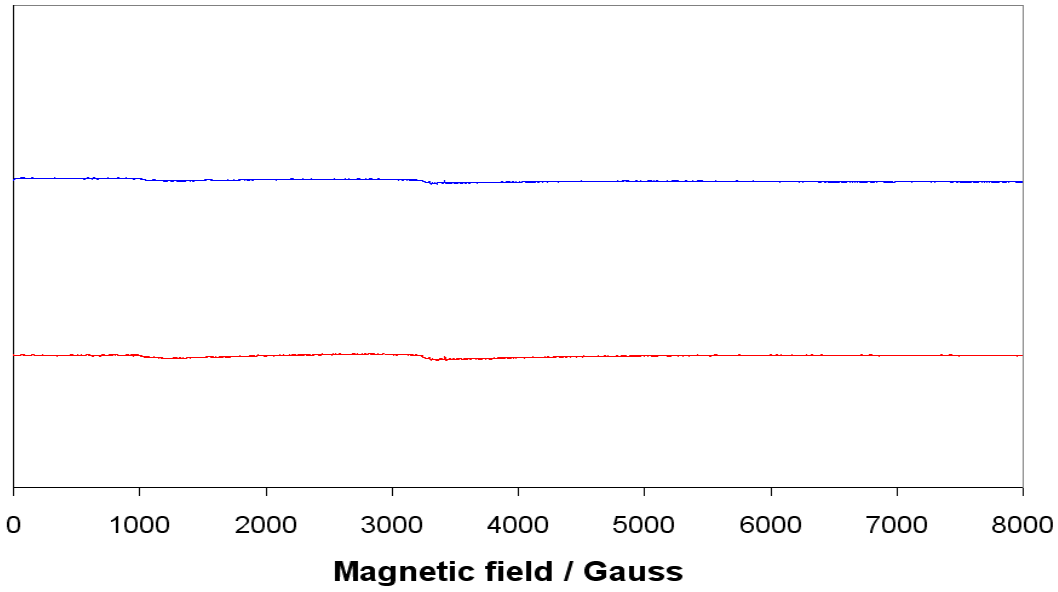

Figure 6. X-band EPR spectra of the polycrystalline complexes recorded at 77 K in DMF: **1** (red) and **2** (blue).

Magnetic property

Lanthanide ions in a dinuclear complex can show anti- or ferromagnetic behavior depending on the structural features of the species.[43] To evaluate the nature of the magnetic coupling between the two Sm(III) and Eu(III) ions, magnetic susceptibility measurements as a function of the temperature were carried out on the compound **2**. The $\chi_M T$ vs T plot and the M vs H plot for **2** are shown in **Figures 7**

and **8** respectively. At room temperature the $\chi_M T$ of complex **2** reaches the value of 1.15 emu K mol^{-1}. With a decrease of the temperature, the product $\chi_M T$ continuously decreases and, at low temperature, it tends to 0; these experimental evidences indicate that the ground state of **2** is diamagnetic and that an antiferromagnetic coupling between the two Eu(III) ions exists. The lack of hysteresis width in the M vs H plot and, of a sharp increasing of susceptibility in the low temperature region, suggests that complex **2** exhibits weak magnetic interactions between spins. These data confirm the diamagnetic behavior of **1** and **2** revealed by EPR spectroscopy. The susceptibility and the resulting effective magnetic moment (0.48 B.M. at 5 K to 3.03 B.M. at 300 K, which cannot be explained by spin crossover between S = 0 and 1) indicate monotonic increasing as the temperature increases, and may be ascribed to the deviation from ideally magnetic behavior of pure and single component such as magnetic impurity. Interestingly, it has been found that several symmetrically bridged lanthanide complexes, for example those formed by Gd(III) and Dy(III), are antiferromagnetically coupled.[44]

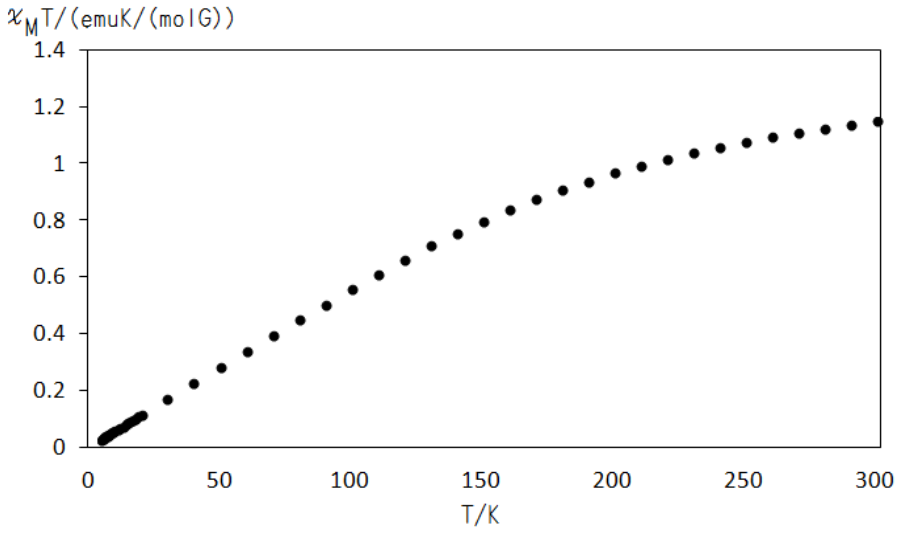

Figure 7. The $\chi_M T$ vs T plot under 0.5 T for **2**.

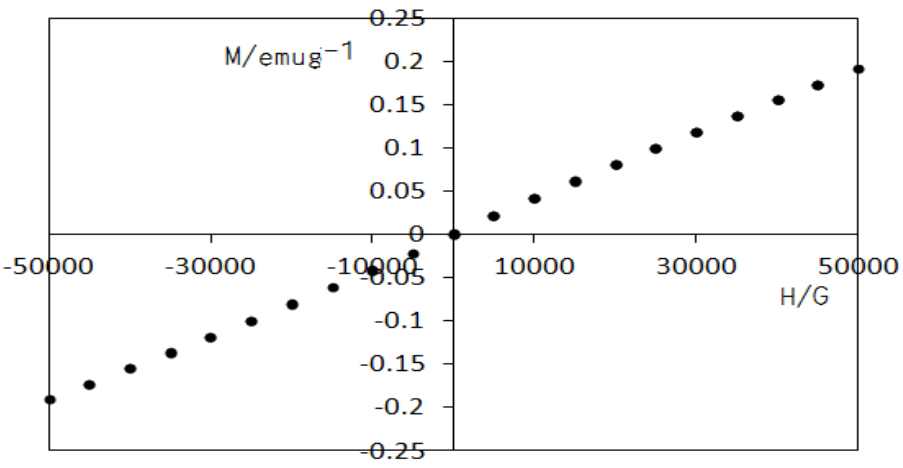

Figure 8. The M vs H plot for the complex at 5 K for **2**.

Biological study

The anti-MRSA activity of the samples by micro-dilution plate methods were examined. In the micro-dilution tests, concentrations of the samples were in the range of 1-512 µg/mL. The MIC (32-128 µg/mL) and MBC (32-128 µg/mL) values against MRSA are given in the **Table 4**. In the anti-mycobacterial sensitivity assay, all compounds were tested against the *M. tuberculosis* H37Rv (ATCC 27294) and the *M. tuberculosis* H37Ra (ATCC 25177) strains, as well as against two clinical strains, strain 1 and strain 2). The results are given in **Table 5**. *M. tuberculosis* H37Rv and *M. tuberculosis* H37Ra are the most commonly used controls for *M. tuberculosis* identification in the drug sensitivity tests.[25] The results showed that all the compounds exhibited anti-mycobacterial activity against all the tested *M. tuberculosis* strains, with MIC and MBC values in the range 2-64 µg/ml and 8-128 µg/ml, respectively. All compounds showed anti bactericidal activity, showing showing a considerable efficacy against the Mycobacteria strains. The mycobacteria cell wall includes a large

amount of complex lipids, lipopolysaccharides and mycolic acids. This constitution makes the cell wall a strong, hydrophobic barrier against antimicrobial agents.[45,46] According to the IC_{50} values reported in **Table 6**, the ligand H_3L was the most effective compound against the three cancer lines (A549, MCF-7 and Caco-2). On the contrary, **2** showed a desirable effect only against the A549 cell line. The IC_{50} value of **1** showed its lack of activity against MCF-7 cells but strong effectiveness on the A549 and Caco-2 cell lines. Among these three compounds, **1** was the least effective considering the IC_{50} value. It was observed that H_3L, **1** and **2** had caused a decrease in the mitochondrial activity by means of the WST-1 assay applied to 3T3, A549, MCF-7 and Caco-2 in the IC_{50} (µg/mL). In particular, complex **1** was very effective against the A549 and Caco-2 cell lines but showed no or little effect against MCF-7 and 3T3.

Table 4. Anti-MRSA activity

	MIC(µg/mL)	MBC(µg/mL)
H_3L	128	128
1	32	32
2	128	128

Table 5.

Anti-mycobacterial activity of samples as MIC and MBC (μg/mL).

	Antimycobacterial activity							
	H37Rv		H37Ra		Strain 1		Strain 2	
	MIC	MBC	MIC	MBC	MIC	MBC	MIC	MBC
H_3L	32	32	32	32	8	32	16	32
1	16	16	8	16	2	8	8	16
2	64	128	64	128	4	16	32	64
Streptomisin	0.65	0.65	0.65	1.29	2.59	5.18	0.65	-
İsoniazid	0.13	1.03	0.51	1.03	0.51	1.03	0.51	0.51
Rifampin	0.65	5.18	0.32	2.59	0.65	0.65	0.65	5.18
Ethambutol	3.74	7.48	1.87	1.87	3.74	3.74	1.87	-

Table 6. IC_{50} values of **H_3L**, complexes **1** and **2** on A549, MCF-7 and Caco-2 cell lines calculated by WST-1 method.

		IC 50 (µg/ml)	
Cell line	**H_3L**	**1**	**2**
3T3	402.41	471.37	>500
A549	15.69	34.6	427.17
MCF-7	119.1	>500	>500
Caco-2	118.87	61.08	>500

Docking study with enoyl acyl carrier protein reductase of *M.Tuberculosis* H37Rv

In view of the world wide spread of multidrug-resistant *M. Tuberculosis* (MDR-TB) and extensively drug-resistant TB (XDR-TB), there is an urgent need to discover antituberculosis medicine of sustainable activity.[47] InhA, the enoyl acyl carrier protein reductase (ENR) from *M. tuberculosis*, is one of the key enzymes involved in the mycobacterial fatty acid elongation cycle and has been validated as an effective antimicrobial target. Isoinazide is a well known tuberculosis drug that binds in the pocket of the enoyl acyl carrier protein reductase and inhibits the action of the fatty acid synthase. In the present study we have docked H_3L and have compared our results with the docking results of the known drug isoniazide with the enoyl acyl carrier protein reductase of mycobacterium tuberculosis. The crystallographic structure of the enoyl acyl carrier protein reductase of *M.Tuberculosis* H37Rv which was downloaded from RCSB protein data bank (PDB ID: 4U0K) was resolved at 1.90

Å. The energy minimized structures of the ligand (H_3L) and isoniazide were used for *in silico* proetin ligand docking studies in the cavity of the protein. A total of 19 amino acids (Ile16, Gly96, Phe97, Met99, Pro99, Gln100, Met103, Tyr158, Met161, Thr196, Lue197, Ala198, Met199, Ser200, Ala201, Ala206, Leu207, Ile210, Ile215) were present in the cavity sites and involved in the binding process. The most favored binding mode of the ligand (**Figures 9, 11)** and isoniazide (**Figures 10, 12)** were selected and explained in **Table 7**. In the best docked pose of H_3L, one hydrogen bond is formed with Thr196 (2.03 Å) of the protein while isoniazide formes two H-bonds, one with Thr196 (2.04 Å) and one with Tyr158 (2.03 Å) (**Table 8**). The complex formed between the protein and the small molecule is slightly more stable in the case of isoniazide with respect to H_3L (**Table 7**).

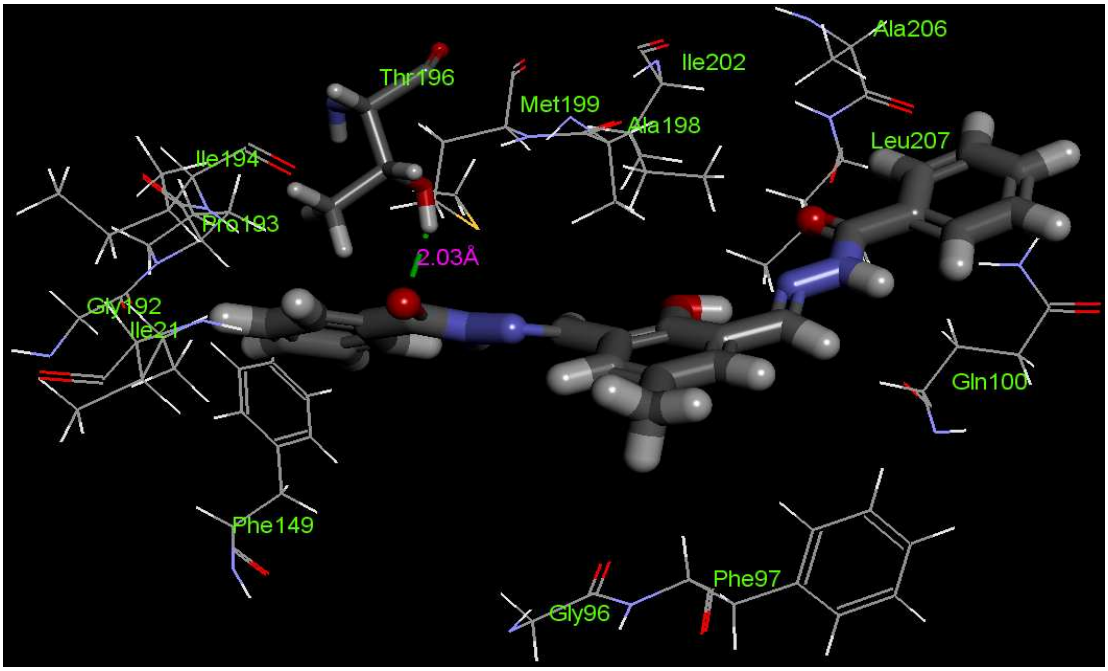

Figure 9. Best docked pose (close view) of H_3L with the enoyl acyl carrier protein reductase (PDB id 4U0K) of *M. tuberculosis* $H37R_v$.

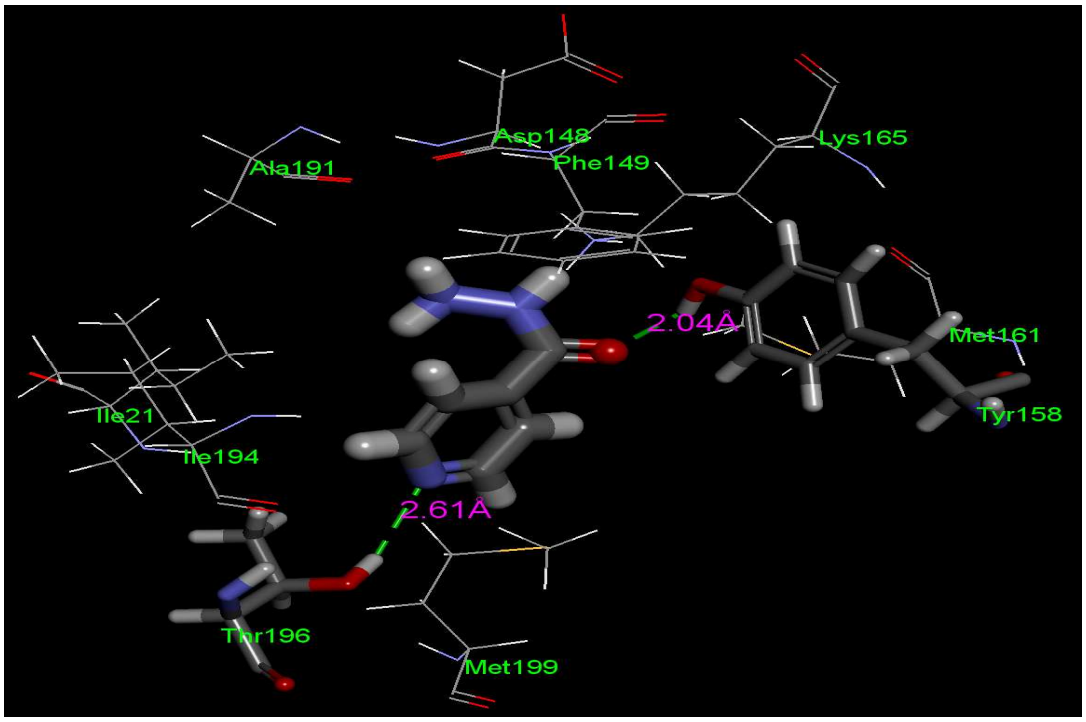

Figure 10. Best docked pose of isoniazide (close view) in the cavity of the enoyl acyl carrier protein reductase (PDB id 4U0K) of mycobacterium tuberculosis H37R$_v$

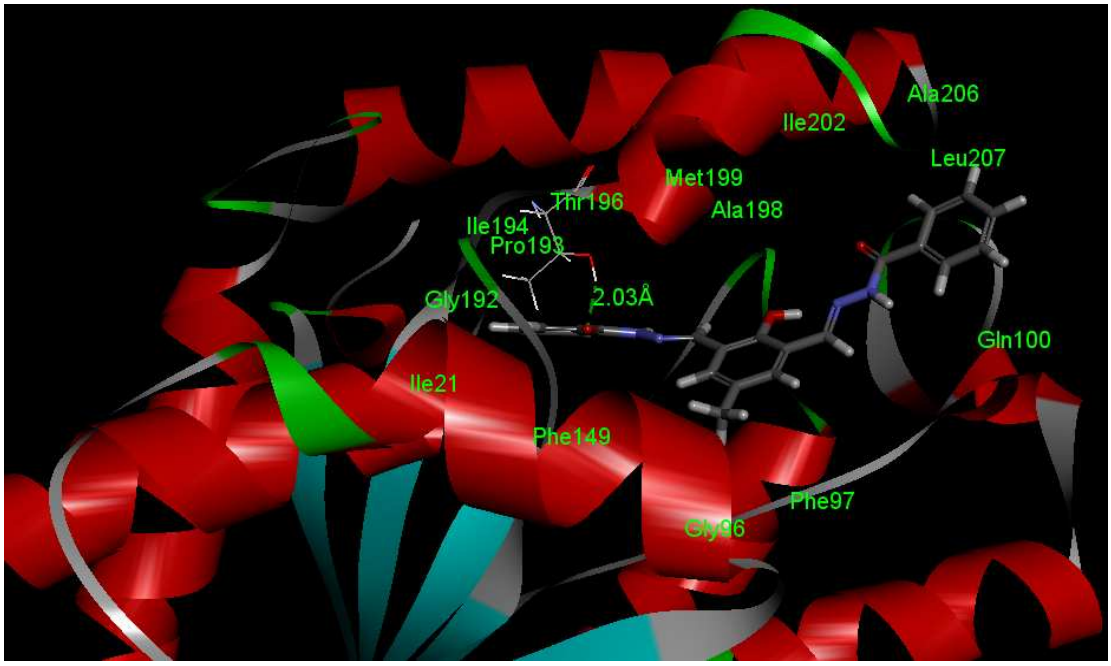

Figure 11. Best docked pose (full view) of H_3L in the cavity of the enoyl acyl carrier protein reductase (PDB id 4U0K) of mycobacterium tuberculosis $H37R_v$

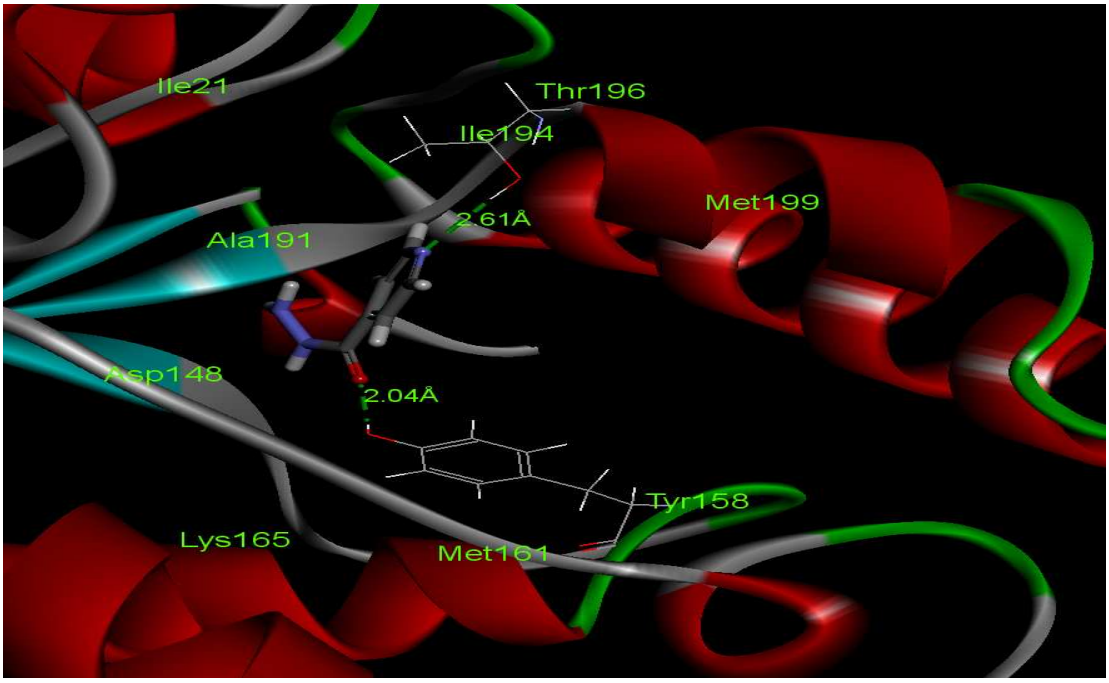

Figure 12. Best docked pose (full view) of isoniazide in the cavity of the enoyl acyl carrier protein reductase (PDB id 4U0K) of mycobacterium tuberculosis $H37R_v$

Table 7. Details of docking studies of H_3L and isoniazide with enoyl acyl carrier protein reductase of *M. Tuberculosis* H37Rv (PDB ID: 4U0K)

Compounds	CDOCKER interaction energy	Binding energy (Kcal/mol)	Ligand energy (Kcal/mol)	Protein energy (Kcal/mol)	Energy of protein ligand complex (Kcal/mol)
4U0K@isoniazide	-16.73	-81.46	3.69	-10272.18	-10349.39
4U0K@ H_3L	-34.48	-84.16	14.89	-10272.18	-10341.45

$Energy_{Binding} = Energy_{Complex} - Energy_{Ligand} - Energy_{Receptor}$

Table 8. Details of the interactions taking place in the most stable protein-ligand complex for H_3L and isoniazide.

Compounds	Hydrogen bonds			
	No. of hydrogen bonds	End 1	End 2	Bond Distances, Å
isoniazide	2	Tyr158	O-atom of isoniazide	2.04
		Thr196	N-atom of pyridine moeity of isoniazide	2.61
H_3L	1	Thr196	O-atom of one of the O=C-NH group of H_3L	2.03

Druglikeness and ADMET prediction

The druglikeness of H_3L was checked following Lipniski's rule of five. The ADMET modules of Discovery Studio were used to check the ADMET (absorption, distribution, metabolism, excretion and toxicity) property of the compounds. Toxicity prediction, aqueous solubility, Blood Brain barrier penetration, Human Intestinal Absorption, and Ames Mutagenicity were predicted under the Calculate Molecular Property module of the Small molecule tool of Discovery Studio client 4.0. The predicted data are summarized in **Table 9**. According to these predictions, compound H_3L is well absorbed and non mutagenic, as opposed to the mutagenic isoniazide.

Table 9. ADMET prediction of H_3L and isoniazide.

Compounds	Molecular Weight	ADMET Solubility (aqueous)	ADMET solubility level	ADMET absorption level≠	ADMET_A logP98	No of H-bond acceptor	No. of H- bond donor	Lipniski's filter	Drug likeness inference	Ames Prediction
Isoniazide	137	-0.033	4	0 (good)	-0.811	2	3	yes	yes, optimal	mutagen
H_3L	400	-4.33	2	0 (good)	3.781	3	5	yes	yes, low	non-mutagen

Conclusions

A binucleating ligand consisting of multidentate sites has been synthesized and its corresponding lanthanide complexes, $[Sm_2(HL)_3]$ (**1**) and $[Eu_2(HL)_3]$ (**2**) (H_3L, 2,6-diformyl-4-methylphenol-di(benzoylhydrazone)) were afforded. Both the complexes were well characterized by different spectral analyses. Additionally, complex **2**, $[Eu_2(HL)_3$ is confirmed by single crystal diffraction technique. In particular, the VTM study confirms the existence of Eu(III)-O-Eu(III) antiferromagnetic coupling. Both the compounds show moderate anti-mycobacterial activity on H37Rv (ATCC 27294) and H37Ra (ATCC 25177) strains. On cytotoxicity study, the ligand and complexes respond well on cancel cell lines (A549, MCF-7 and Caco-2), however; complex **1** is little toxic on healthy cell line like 3T3. In summary, the studies here reported have evidenced the presence of a new class of lanthanide complexes with potential use in the biomedical field, and further investigations in this area are currently being carried out in our laboratories.

Supplementary materials

Crystallographic data (excluding structure factors) for the structure reported have been deposited with the Cambridge Crystallographic Data Centre as supplementary publication no. CCDC-874020 for **2** and can be obtained free of charge on application to the CCDC, 12 Union Road, Cambridge, CB2 IEZ, UK (fax: +44-1223-336-033; e-mail deposit@ccdc.cam.ac.uk or http://www.ccdc.cam.ac.uk).

Acknowledgements

KD and CS would like to thank West Bengal DST, Kolkata, India for the grant (228/1(10)/(Sanc.)/ST/P/S&T/9G-16/2012). AD would like to thank to The Scientific & Technological Research Council of Turkey (TÜBITAK) for the grant (2221 – Fellowship for Visiting Scientist).

References

[1] (a) A. Bianchi, K. Bowman-James, E. Garcia-Espana, E. *Supramolecular Chemistry of Anions*; Wiley-VCH: New York, 1997; (b) A. E. Martell, D. T. Sawyer, *Oxygen Activation by Transition Metals*; Plenum Press: New York, 1987; (c) J. M. Lehn, *Supramolecular Chemistry. Concepts and Perspectives*; VCH: Weinheim, Germany, 1995.

[2] (a) H. S. Park, Q. Lin, A. D. Hamilton, *Proc. Natl. Acad. Sci. U.S.A*. 2002, **99**, 5105-5110; (b) M. J. Hannon, V. Moreno, M. J. Prieto, E. Moldrheim, E. Sletten, I. Meistermann, C. J. Isaac, K. J. Sanders, A. Rodger, *Angew. Chem. Int. Ed*. 2001, **40**, 879-884.

[3] E. Deiters, B. Song, A. Chauvin, C. D. B. Vandevyver, F. Gumy, J. G. Bunzli, *Chem. Eur. J.* 2009, **15**, 885-900; (b) T. V. Balashova, N. A. Belova, M. E. Burin, D.M. Kuzyaev, R. V. Rumyantcev, G. K. Fukin, A. P. Pushkarev, V. A. Ilichev, A. F. Shestakov, I. D. Grishin M. N. Bochkarev *RSC Adv.*, 2014,**4**, 35505–35510 ; (c) A. W. Woodward, A. Frazer, A. R. Morales, J.Yu, A. F. Moore, A.D. Campiglia, E.V. Jucov, T. V. Timofeeva, K. D. Belfield *Dalton Trans*. 2014, DOI: 10.1039/C4DT01507J.

[4] (a) V. Alexander, *Chem. Rev*. 1995, **95**, 273-342; (b) F. B. Han, Y. L. Zhang, X. L. Sun, B. G. Li, Y. H. Guo, Y. Tang, *Organometallics* 2008, **27**, 1924-1928; (c) X. H. Yang, X. L. Sun, F.B. Han, B Liu, Y. Tang, C. Wang, M. L. Gao, Z. W. Xie, S. Z. Bu, *Organometallics* 2008, **27**, 4618-4624; (d) C. Wang, Z. Ma, X. L. Sun, Y. Gao, Y. H. Guo, Y. Tang, L. P. Shi, *Organometallics* 2006, **25**, 3259-3266..

[5] (a) E. Grunova, E. Kirillov, T. Roisnel, J. F. Carpentier, *Organometallics* 2008, **27**, 5691-5698; (b) G. Zi, X. Li, H. Song, *Organometallics* 2008, **27**, 1242-1246; (c) Q. Wang, L. Xiang, H. Song, G. Zi, *Inorg. Chem*. 2008, **47**, 4319-4328; (d) L. Xiang, Q. Wang, H. Song, G. Zi, *Organometallics* 2007, **26**, 5323-5329; (e) S. A. Schuetz, C. M. Silvernail, C. D.Incarvito, A.L.Rheingold, J. L. Clark, V. W. Day, J. A. Belot, *Inorg. Chem*. 2004, ***43***, 6203-6214.

[6] (a) P. M. Zeimentz, S. Arndt, B. R. Elvidge, J. Okuda, *Chem. Rev*. 2006, **106**, 2404-2433; (b) L. Bourget-Merle, M. F. Lappert, J. R. Severn, *Chem. Rev*. 2002, **102**, 3031-3066.

[7] (a) X. C. Zhu, J. X. Fan, Y. J. Wu, S. W. Wang, L. J. Zhang, G. S. Yang, Y. Wei, C. W. Yin, H. Zhu, S. H. Wu, H. T. Zhang, H. T. *Organometallics* 2009, **28**, 3882-3888; (b) Y. J. Wu, S. W. Wang, X. C. Zhu, G. S. Yang, Y. Wei, L. J. Zhang, H. B. Song, H. *Inorg. Chem*. 2008, **47**, 5503-5511; (c) L. Y. Zhou, Y. M. Yao, C. Li, Y. Zhang, Q. Shen, *Organometallics* 2006, *25*, 2880-2885; (d) K. C. Hultzsch, F. Hampel, T. Wagner, *Organometallics* **2004**, **23**, 2601-2612.

[8] (a) H. E. Dyer, S. Huijser, N. Susperregui, F. Bonnet, A. D. Schwarz, R. Duchateau, L. Maron, P. Mountford, *Organometallics* 2010, **29**, 3602-3621; (b) Z. J. Zhang, X. P. Xu, S. Sun, Y. M. Yao, Y. Zhang, Q. Shen, *Chem. Commun*. 2009, 7414-7416.

[9] (a) S. P. Summers, T. K. A. Abboud, W. S. Brey, B. Bechtel, R. C. Palenik, G. J. Palenik, *Polyhedron* 1996, **15**, 3101-3106; (e) M. Diop, F. B. Tamboura, M. Gaye, A. S. Sall, A. H. Barry, T. Jouini, *Inorg. Chem. Commun*. 2003, **6**, 1004-1010; (f) F. B. Tamboura, P. M. Haba, M. Gaye, A. S. Sall, A. H. Barry, T. Jouini, *Polyhedron* 2004, **23**, 1191-1197; (g) U. Abram, A. Jagst, A.

Sanchez, E. M. Vázquez-López, *Inorg. Chem*. 2005, **44**, 5738-5744; (h) S.-Y. Lin, G.-F. Xu, L. Zhao, Y.-N. Guo, Y. Guo and J. Tang *Dalton Trans.*, 2011, **40**, 8213–8217.

[10] (a) J. Kido, Y. Okamoto, *Chem. Rev*. 2002, **102**, 2357-2368; (b) W. G. Quirino, R. D. Adati, S. A. M. Lima, C. Legnani, M. Jafelicci, M.R. Davolos, M. Cremona, *Thin Solid Films* 2006, **515**, *927*-931.

[11] W. Szuszkiewicz, B. Keller, M. Guzik, T. Aitasalo, J. Niittykoski, J. Hölsä, J. Legendziewicz, *J. Alloys Compd*. 2002, **341**, 297-306.

[12] R. Robson, *Inorg. Nucl. Chem. Lett*. 1970, **6**, 125-128; (b) R. Robson, *Aust. J. Chem*. 1970, **23**, 2217-2224.

[13] B. F. Hoskins, R. Robson, H. Schaap, *Inorg. Nucl. Chem. Lett*. 1972*,* **8***,* 21-25.

[14] (a) C. Edder, C. Piguet, J. C. G. Bunzli, G. Hopfgartner, *Chem. Eur. J*. 2001, **7**, 3014-3024; (b) S. I. Klink, H. Keizer, F. van Veggel, *Angew. Chem., Int. Ed*. 2000, **39**, 4319-4321; (c) D.Banerjee, Z. Hu, J. Li *Dalton Trans.* 2014, **43**, 10668–10685.

[15] (a) M. Albrecht, O. Osetska, R. Fröhlich, *Dalton Trans*. 2005, 3757-3762; (b) R. W. -Y. Sun, D. -L. Ma, E. L. -M. Wong, C. -M. Che, *Dalton Trans*. 2007, 4884-4892.

[16] A. L. Okunade, M. P. F. Elvin-Lewis, *Phytochem*. 2004, **65**, 1017-1032.

[17] N. Lall, M. D. Sarma, B. Hazra, J. J. Meyer, *J. Antimicro. Chemo*. 2003, **51**, 435-438.

[18] E. Banfi, M. G. Mamolo, D. Zampieri, L. Vio, C. M. Bragadin, *J. Antimicro. Chem*. 2001, **48**, 705-712.

[19] (a) M. Sakamoto, S. Itose, T. Ishimori, N. Matsumoto, H. Ōkawa, S. Kida, *Dalton Trans*. 1989, 2083-2089; (b) M. Sakamoto, S. Itose, T. Ishimori, N. Matsumoto, H. Ōkawa, S. Kida, *Bull. Chem. Soc. Japan* 1990, **63**, 1830-1831.

[20] D. F. Eaten, *Pure & Appl. Chem*. 1988, **60**, 1107-1114.

[21] WINEPR SimFonia, version 1.25, Bruker Analytische Messtechnik GmbH, Karlsruhe, 1996.

[22] E. W. Koneman, S. D: Allen, W. M. Janda, P. C. Schreckenberger, *Mycology*. 1997, **5**, 983-1069.

[23] NCCLS. Methods for Determining Bactericidal Activity of Antimicrobial Agents; Approved Guideline, NCCLS document M26-A [ISBN 1-56238-384-1]. NCCLS, 940 West Valley Road, Suite 1400, Wayne, Pennsylvania 19087 USA, 1999.

[24] B. D. Becton, Dickinson and Company Newsletter BD (2002). Bactec MGIT 960 SIRE kit now FDA-cleared for susceptibility testing of Mycobacterium tuberculosis. *Microbiology News & Ideas* 13, 4.

[25] NCCLS (2003). National Committee for Clinical Laboratory Standards (NCCLS). Susceptibility Testing of Mycobacteria, Nocardiae, and Other Aerobic Actinomycetes; Approved Standard. NCCLS document M24-A [ISBN 1-56238-500-3]. NCCLS, 940 West Valley Road, Suite 1400, Wayne, Pennsylvania 19087-1898 USA, 2003.

[26] NCCLS (2006). National Committee for Clinical Laboratory Standards (NCCLS). National Committee for Clinical Laboratory Standards. Methods for Dilution Antimicrobial Susceptibility Tests for Bacteria That Grow Edition Aerobically; Approved Standard. Seventh Edition NCCLS Document M7-A7., Wayne, Pennsylvania 2006, **26**(2), 1-16.

[27] C. A. Lipinski, F. Lombardo, B. W. Dominy, P. J. Feeney, *Adv. Drug Delivery Rev*. 2001, **46**, 3-26.

[28] C. A. Lipinski, *Drug discovery today: Technologies*. 2004, **1**, 337-341.

[29] Discovery Studio 4.0 is a product of Accelrys Inc, San Diego, CA, USA.

[30] (a) SADABS Bruker AXS; Madison, Wisconsin, USA, 2004; SAINT, *Software Users Guide*, *Version 6.0*; Bruker Analytical X-ray Systems, Madison, WI, 1999; (b) G. M. Sheldrick, SADABS v2.03: *Area-Detector Absorption Correction*. University of Göttingen, Germany, 1999.

[31] A. Altomare, M. C. Burla, M. Camalli, G. L. Cascarano, C. Giacovazzo, A. Guagliardi, A. G. G. Moliterni, G. Polidori, R. Spagna, *J. Appl. Crystallogr.* 1999, **32**, 115-119.

[32] G. M. Sheldrick, *Acta Cryst.* A 2008, **A64**, 112-122.

[33] L. J. Farrugia, *J. Appl. Crystallogr*. 1999, **32**, 837-838.

[34] K. Nakamoto, Infrared and Raman Spectra of Inorganic and Coordination Compounds, Parts A and B, 5th Ed., John Wiley, New York, 1997.

[35] (a) F. B.Tamboura, O. Diouf, A. H.Barry, M. Gaye, A. S. Sall, *Polyhedron*, 2012, **43**, 97-103; (b) T. Mistri, M. Dolai, D. Chakraborty, A. R. Khuda-Bukhsh, K. K. Das, M. Ali, *Org.Biomol.Chem*., 2012, **10**, 2380-2384; (c); S.-Y. Lin, G.-F. Xu, L. Zhao, Y.-N. Guo, Y. Guo, J. Tang, *Dalton Trans*., 2011, **40**, 8213- 8217; (d) Y. Shiping, C. Peng, L. Daizheng, J. Zonghui, W. Genglin, W. Honggen, Y. Xinkan, Polyhedron, 1992, **11**, 879-883.

[36] A. B. P. Lever, Inorganic Electronic Spectroscopy, 2nd Ed., Elsevier, New York, 1984.

[37] (a) Y. -H. Zhang, X. Li, S. Song, H. -Y. Yang, D. Ma, Y. -H. Liu, *Cryst. Eng. Comm.* 2014, **16**, 8390–8397; (b) L. Liu, M. S. Alam, D. -U. Lee, *Bull.*

Korean Chem. Soc. 2012, **33**, 3361-3367; (c) E. Bakier, M. S. A. Abdel-Mottaleb, *Int. J. Photoenergy*. 2005, **7**, 51-58.

[38] (a) S. Faulkner, S. J. A. Pope, B. P. Burton-Pye, *Applied Spec. Review* 2005, **40**, 1-31. (b) Q. Li, T. Li, J. Wu, *J. Phys. Chem. B* 2001**, 105***,* 12293-12296.

[39] B.Valuer, Molecular Fluorescence: Principles and Applications, Wiley-VCH, Weinheim, 2001.

[40] K. Thompson, S. K. Mandal, S. S. Tandon, J. N. Bridson, M. K. Park, *Inorg. Chem*. 1996, **35**, 3117-3125.

[41] V. H. Crawford, H. W. Richardson, J. R. Wasson, D. J. Hodgsin, W. E. Hatfield, *Inorg. Chem*. 1976, **15**, 2107-2110.

[42] (a) S. Thakurta, J. Chakraborty, G. Rosair, J. Tercero, M. S. El Fallah, E. Garribba, S. Mitra, *Inorg. Chem*. 2008, **47**, 6227-6235; (b) S. Thakurta, P. Roy, G. Rosair, C. J. Gómez-García, E. Garribba, S. Mitra, *Polyhedron* 2009, **28**, 695-702; (c) A. Ray, S. Mitra, A. Dehno Khalaji, C. Atmani, N. Cosquer, S. Triki, J. M. Clemente-Juan, S. Cardona-Serra, C. J. Gómez-García, R. J. Butcher, E. Garribba, D. Xu, *Inorg. Chim. Acta* 2010, **363**, 3580-3588.

[43] F. Habib, M. Murugesu, *Chem. Soc. Rev.* 2013, **42**, 3278-3288.

[44] (a) L. E. Roy, T. Hughbanks, *J. Am. Chem. Soc*. 2006, **128**, 568-575; (b) P.-H. Lin, T. J. Burchell, R. Clérac, M. Murugesu, *Angew. Chem. Int. Ed*. 2008, **47**, 8848 –8851.

[45] D. E. Minnikin, M. Goodfellow, 1980, 189. In Microbiological classification and identification; Goodfellow, M., Board, R. G., Eds.; Academic: London.

[46] D. E. Minnikin, 1982, 95. Lipids; compiex iipids, their chemistry, biosynthesis and roles. In The biology of mycobacteria. Ratledge, C, and Stanford, J. (eds).; Academic Press, London.

[47] A. Zumla, P. Nahid, S. T. Cole, *Nat. Rev. Drug Discov*. 2013, **12**, 388-404.